

DEVICE TECHNOLOGY

Precise pitch-scaling of carbon nanotube arrays within three-dimensional DNA nanotrenches

Wei Sun^{1,2,*}, Jie Shen^{1,2,†}, Zhao Zhao^{1,3,4,†}, Noel Arellano⁵, Charles Rettner⁵, Jianshi Tang⁶, Tianyang Cao¹, Zhiyu Zhou¹, Toan Ta⁵, Jason K. Streit⁷, Jeffrey A. Fagan⁷, Thomas Schaus^{1,2}, Ming Zheng⁷, Shu-Jen Han⁶, William M. Shih^{1,3,4}, Hareem T. Maune⁵, Peng Yin^{1,2,*}

Precise fabrication of semiconducting carbon nanotubes (CNTs) into densely aligned evenly spaced arrays is required for ultrascaled technology nodes. We report the precise scaling of inter-CNT pitch using a supramolecular assembly method called spatially hindered integration of nanotube electronics. Specifically, by using DNA brick crystal-based nanotrenches to align DNA-wrapped CNTs through DNA hybridization, we constructed parallel CNT arrays with a uniform pitch as small as 10.4 nanometers, at an angular deviation $<2^\circ$ and an assembly yield $>95\%$.

Although conventional transistor lithography successfully scales the channel pitch (spacing between two adjacent channels within individual transistor) of bulk materials (that is, Si), the performance drops for patterning one-dimensional (1D) semiconductors, such as carbon nanotubes (CNTs), at ultrascaled technology nodes (1, 2). The projected channel pitches [~ 10 nm or less (1)] for multichannel CNTs are smaller than the fabrication feasibility of current lithography. Alternatively, thin-film approaches (1), which use physical forces (3–6), or chemical recognition (7–9) to assemble CNTs, provide a density exceeding 500 CNTs/ μm (3). However, assembly defects, including crossing (4, 10), bundling (i.e., multiple CNTs aggregated side by side) (3), and irregular pitches (11), are widely observed in such CNT thin films.

Structural DNA nanotechnology (12, 13), in particular DNA origami (14, 15) and DNA

bricks (16, 17), can produce user-prescribed 2D or 3D objects at 2-nm feature resolution. Self-assembled DNA structures have been used to pattern diverse materials, including oxides (18, 19), graphene (20), plasmonic materials (21, 22), polymers (23), and CNTs (8, 9, 24, 25). Despite these demonstrations, unconfined surface rotation (8, 24) still limits the precise pitch scaling achieved within a DNA template. Additionally, CNT arrays assembled by using double-stranded DNAs (dsDNAs) (8) contain only a small number of CNTs per single-orientation domain (2.4 on average), less than the desired value of six CNTs (1).

By using nanotrenches based on DNA brick crystals to spatially confine the DNA hybridization-mediated CNT alignment, we developed a spatially hindered integration of nanotube electronics (SHINE) method for building evenly spaced CNT arrays (Fig. 1). DNA hybridizations between single-stranded handles within the nanotrenches and the anti-

handles (sequences complementary to the DNA handles) on CNTs compensated for the electrostatic repulsions during assembly. DNA nanotrenches also confined the orientation of individual CNTs precisely along their longitudinal axis.

Programming the DNA trench periodicity thus rationally scaled the inter-CNT pitch from 24.1 to 10.4 nm. Misaligned CNTs could not access the DNA handles and were repelled from the DNA templates by electrostatic repulsion. The pitch precision, indicative of array uniformity, improved when compared to the values for CNT thin films (11). The design for SHINE began by constructing parallel nanotrenches along the x direction (Fig. 1). The feature-repeating unit of DNA brick crystal template (17) contained 6768 base pairs. The sidewall and the bottom layer within the unit consisted of 6 helices by 8 helices by 94 base pairs and 6 helices by 4 helices by 94 base pairs along the x and y and z directions, respectively. At the top surface of the bottom layer, we introduced four 14-nucleotide (nt) single-stranded DNA (ssDNA) handles by extending the 3' or 5' ends of four selected DNA bricks (fig. S14) (26). Extending the repeating units along the

¹Wyss Institute for Biologically Inspired Engineering, Harvard University, Boston, MA 02115, USA. ²Department of Systems Biology, Harvard Medical School, Boston, MA 02115, USA. ³Department of Cancer Biology, Dana-Farber Cancer Institute, Harvard Medical School, Boston, MA 02115, USA. ⁴Department of Biological Chemistry and Molecular Pharmacology, Harvard Medical School, Boston, MA 02115, USA. ⁵IBM Almaden Research Center, San Jose, CA 95120, USA. ⁶IBM Thomas J. Watson Research Center, Yorktown Heights, NY 10598, USA. ⁷Materials Science and Engineering Division, National Institute of Standards and Technology (NIST), Gaithersburg, MD 20899, USA.

*Corresponding author. Email: py@hms.harvard.edu (P.Y.); sunwedavid1@gmail.com (W.S.) †These authors contributed equally to this work.

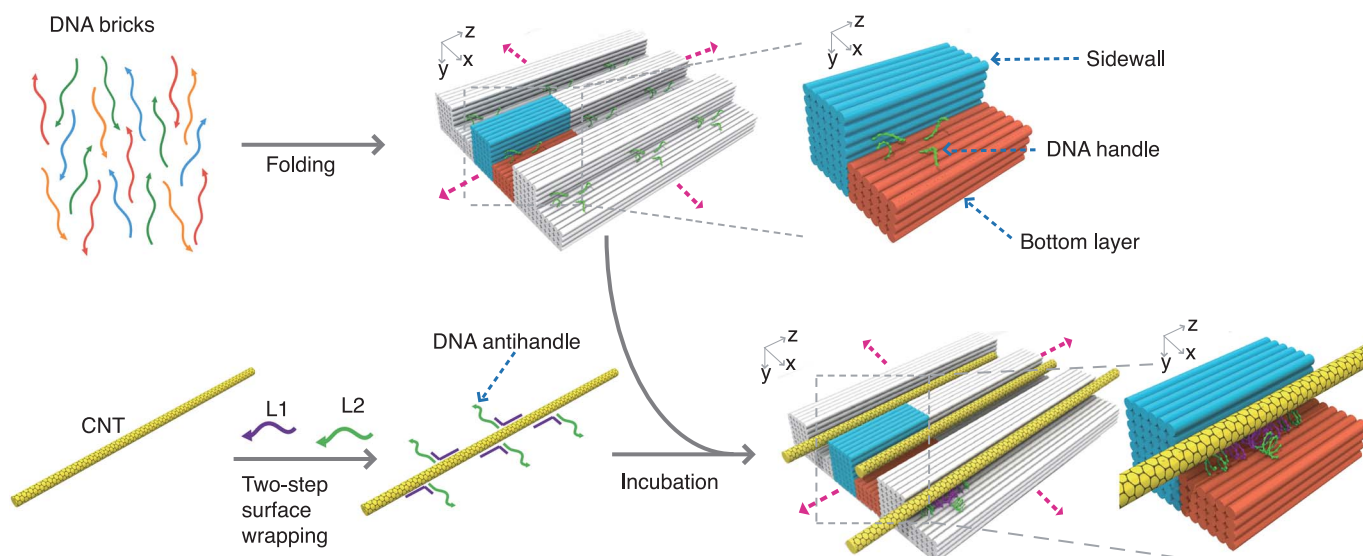


Fig. 1. Design schematic for SHINE. The blue and the orange bundles represent the sidewall and the bottom layer, respectively, within a feature-repeating unit of trench-like DNA templates. Pink arrows indicate the extension directions of the repeating units.

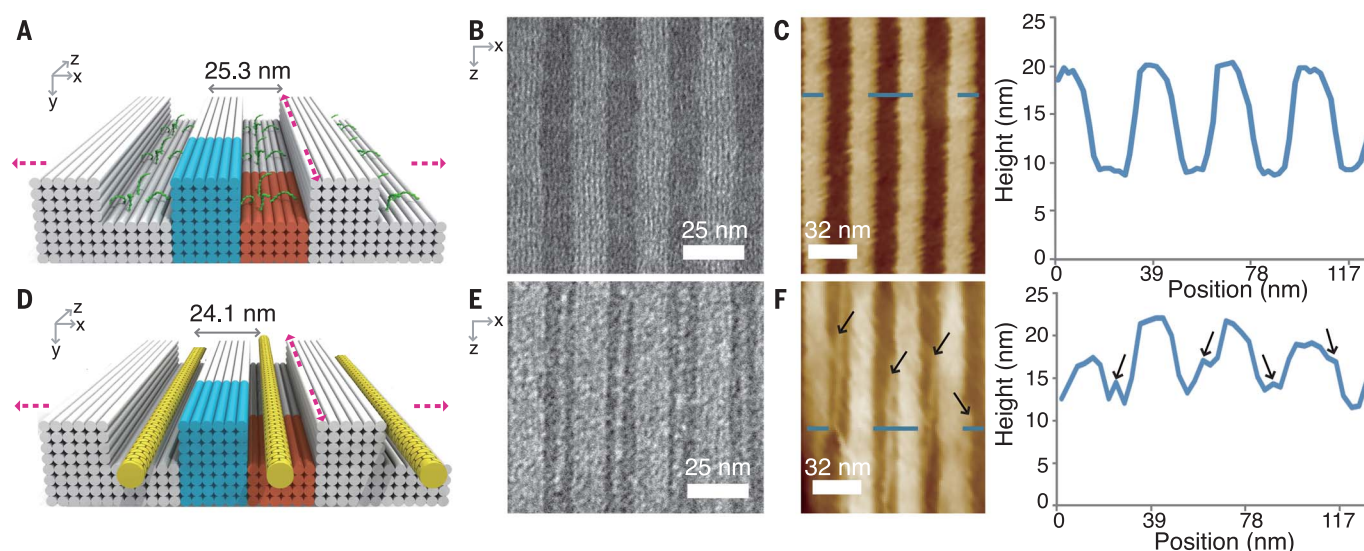


Fig. 2. Assembling CNT arrays with 24-nm inter-CNT pitch. From left to right, designs (A and D), zoomed-in TEM images along the x and z projection direction (B and E), liquid-mode AFM images along the x and z projection direction (C and F) (left), and height profiles (C and F) (right) for the DNA template (A to C) and the assembled CNT array (D to F),

respectively. Blue dashed lines [in (C) and (F), left] represent the locations for the height profile. Black arrows in the AFM image (F) indicate the assembled CNTs. See also figs. S2 to S4, S16, and S17 (26). The orientation of the assembled CNTs in (F) may be distorted by AFM tips during imaging.

x and z directions yielded DNA templates with parallel nanotrenches.

The micrometer-scale DNA templates were folded through a multistage isothermal reaction. Next, DNA antihandles were wrapped onto CNTs through noncovalent interactions (fig. S1) (27, 28). Finally, under mild conditions, the hybridization between the DNA handles and the antihandles mediated CNT assembly within the DNA nanotrenches at the prescribed inter-CNT pitch.

Transmission electron microscopy (TEM) imaging confirmed the successful formation of the designed DNA templates (Fig. 2, A and B, and figs. S2 to S4) (26), as well as the confined assembly of evenly spaced CNT arrays within the DNA nanotrenches (Fig. 2, E and F, and figs. S16 and S17). In the zoomed-out TEM images (figs. S2 and S3), the assembled DNA templates exhibited wide dimensional distributions. One typical DNA template (fig. S2C) exhibited the maximal dimensions of $1.3\ \mu\text{m}$ by $200\ \text{nm}$ in the x and z directions. In the zoomed-in TEM images, DNA templates exhibited alternative dark (bottom layer)—bright (sidewall) regions (Fig. 2B and fig. S17), and each region corresponded to six-layered DNA helices along the x direction as designed (Fig. 2A). The measured nanotrench periodicity was $25.3 \pm 0.3\ \text{nm}$ ($N = 50$ nanotrenches from 10 different templates) along the x direction after drying on the surface (corresponding to $2.1\ \text{nm}$ diameter per dehydrated dsDNA). The ssDNA handles were not visible in the negatively stained TEM images.

After CNT assembly, we found bright parallel lines that appeared exclusively on the dark

bottom regions, indicative of the aligned CNTs along the longitudinal axis of the nanotrenches (Fig. 2, D and E, and figs. S16 and S17). The relatively larger diameter of CNTs as compared with the unwrapped CNTs was caused by the stained dsDNA layer around CNTs (fig. S15). Despite a few local twists in individual CNTs, we did not observe crossing or bundling CNT defects within the DNA nanotrenches. The measured inter-CNT pitch was $24.1 \pm 1.7\ \text{nm}$ ($N = 50$ CNTs from 10 different templates). For every two neighboring CNTs, we measured three different positions along the longitudinal axis of CNT. Slightly smaller inter-CNT pitch, compared to the x -direction periodicity of the DNA templates, was the result of statistical variance of the small sample size. The integrity of the DNA templates was not affected by CNT assembly, as indicated by the consistent six-layered DNA helices (along the x direction) in both the DNA sidewall and bottom layer (Fig. 2E).

To evaluate the pitch precision, we calculated (i) the standard deviation, (ii) the range value, (iii) the percent relative range, and (iv) the index of dispersion for count value (IDC value) for inter-CNT pitch. The range of inter-CNT pitch variation, defined as the difference between the maximum and the minimum pitch values, was $7.8\ \text{nm}$. The percent relative range of the inter-CNT pitch, defined as the range of inter-CNT pitch divided by the average value of inter-CNT pitch ($24.1\ \text{nm}$), was 32% . For comparison, on a flat substrate, a range $>30\ \text{nm}$ and a percent relative range $>140\%$ have been reported for CNT arrays with similar average pitch (4).

The IDC value [defined as the standard deviation squared divided by the average pitch squared ($1I$)] for CNT arrays ($\sim 40\ \text{CNTs}/\mu\text{m}$) from SHINE was 0.005 , two orders of magnitude smaller than for CNT arrays of similar density fabricated from thin-film approaches ($1I$). Hence, by limiting the rotation of CNTs with DNA sidewalls, SHINE provided higher precision for assembling ultradense CNT arrays than flat substrate-based assembly. Similarly, SHINE produced a smaller angular deviation (less than 2° , defined as the longitudinal-axis difference between CNTs and the DNA nanotrenches) than previously obtained on flat DNA template, where $>75\%$ CNTs exhibited angular deviations $>5^\circ$ (24).

Because both DNA templates (figs. S2 and S3) and CNTs (fig. S15) exhibited uneven widths and lengths, we observed a variable number of CNTs (ranging from 4 to 15) on different templates, as well as z -direction offset for CNTs from trench to trench (fig. S17). Notably, although the width of the DNA nanotrench ($12\ \text{nm}$) was larger than the diameter of individual CNTs, we did not observe CNT bundling within individual trenches.

We further analyzed the assembly yield of aligned CNTs by TEM counting (supplementary text S2). The assembly yield was defined as the total number of inner nanotrenches occupied by correctly assembled parallel CNT arrays divided by the total number of inner DNA nanotrenches. Partially formed DNA nanotrenches on the boundaries were excluded. A $>95\%$ assembly yield was observed for 10 randomly selected DNA templates (more than 50 inner trenches were counted, Fig. 2E

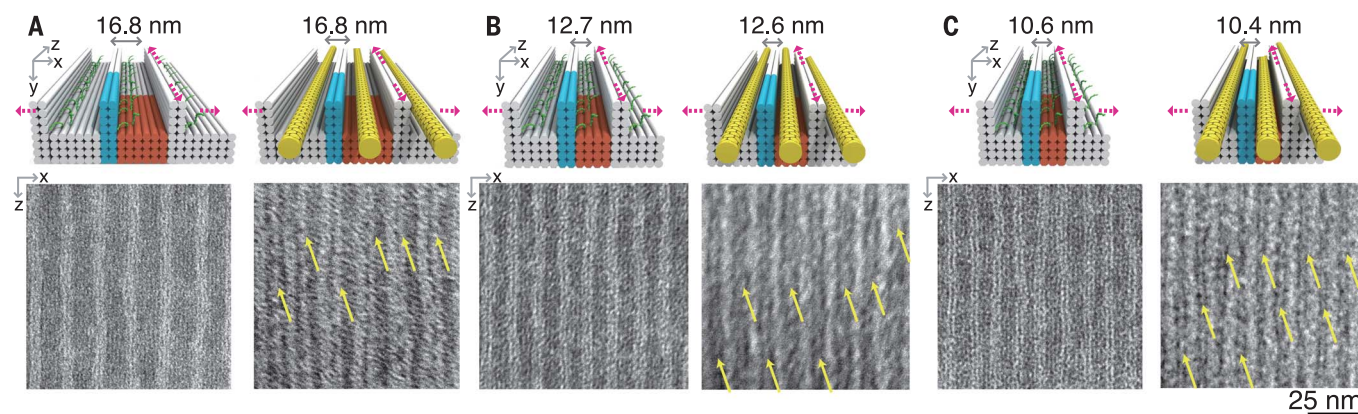


Fig. 3. Programming inter-CNT pitches with DNA brick crystal templates. (A to C) Designs (top row) and zoomed-in TEM images along the x and z projection direction (bottom row) for the DNA templates (left) and the assembled CNT arrays (right) at 16.8 nm (A), 12.6 nm (B), and 10.4 nm (C) inter-CNT pitches, respectively. Yellow arrows in the TEM images indicate the assembled CNTs. See also figs. S6 to S13 for the assembled DNA templates and figs. S19 to S24 for the assembled CNT arrays (26).

and fig. S17), and <5% of inner nanotrenches were unoccupied by CNTs (fig. S25).

In liquid-mode atomic force microscopy (AFM) images (Fig. 2F and fig. S18), we observed new peaks (with heights ~ 15 to 17 nm) within the nanotrenches (fig. S18) after CNT assembly. The height changes of the new peaks (5 to 7 nm), relative to the height of the bottom layer beneath (~ 10 nm in height, Fig. 2C), approximated the sum of dsDNA handle length (3 to 5 nm, depending on different conformations) and DNA-wrapped CNT diameter (~ 1 to 3 nm, fig. S15). Therefore, only single-layer CNTs were assembled. The ssDNA handles were not visible in the AFM images. We observed wider inter-CNT pitch (~ 32 nm) in liquid-mode AFM when compared with that from the TEM images. The pitch change was ascribed to the larger diameter of hydrated dsDNAs (2.6-nm diameter per helix) in liquid condition than of the fully dehydrated dsDNAs (2.1-nm diameter per helix under vacuum). The 32-nm inter-CNT pitch on the hydrated DNA templates could shrink to ~ 24 nm after dehydration under heat.

By programming DNA nanotrenches with different trench periodicities along the x direction, we further demonstrated prescribed scaling of inter-CNT pitches at 16.8, 12.6, and 10.4 nm (Fig. 3). Within the feature-repeating units of the small-periodicity DNA templates, we used 2 helices by 8 helices by 94 base pairs for the nanotrench sidewalls (Fig. 3, A to C, top left). In the bottom layers, 6 helices by 4 helices by 94 base pairs, 4 helices by 4 helices by 94 base pairs, and 3 helices by 4 helices by 94 base pairs were used for different nanotrench periodicities.

We assembled DNA templates and CNT arrays using approaches similar to those in Fig. 1. Assembled DNA templates exhibited measured nanotrench periodicities of 16.8 ± 0.4 nm, 12.7 ± 0.2 nm, and 10.6 ± 0.1 nm ($N = 50$

to 300 nanotrenches from 10 individual templates for each design) along x direction (Fig. 3, A to C, bottom left, and figs. S5 to S13) (26). Notably, we observed slightly twisted nanotrench sidewalls after drying in vacuum, probably because of the relatively low structural stiffness of the two-layer DNA sidewalls (29). However, the average periodicities were not affected by the twisting of the DNA sidewalls. In the zoomed-out view, different template designs showed typical dimensions of ~ 1.3 μm by 300 nm along the x and z directions (figs. S5, S6, S8, S9, S11, and S12).

After CNT assembly, parallel CNTs were aligned within the DNA nanotrenches (designs in Fig. 3, A to C, top right; TEM images in Fig. 3, A to C, bottom right; figs. S19 to S24). The inter-CNT pitches varied from 16.8 ± 1.5 nm to 12.6 ± 0.6 nm to 10.4 ± 0.4 nm, respectively ($N = 50$ to 300 CNTs from 10 individual templates for each design). Both the 10.4-nm pitch value and 0.4-nm standard deviation (smaller than the diameter of individual CNTs) were beyond current lithography-defined channel pitches (30, 31).

The IDC values were 0.008, 0.002, and 0.001, respectively—orders of magnitude smaller than those from thin-film approaches (11) (supplementary text S4.1). The range and the percent relative range of the inter-CNT pitch variation were 5.9 nm and 36%, 2.7 nm and 24%, and 1.9 nm and 18% for 16.8-, 12.6-, and 10.4-nm inter-CNT pitches, respectively. Narrower DNA nanotrenches improved the precision of CNT assembly (fig. S26). When the width of DNA nanotrenches was decreased to ~ 6 nm (in 10.4-nm pitch CNT arrays), the range value of inter-CNT pitch was decreased to <2 nm and the IDC value (0.001) improved by eightfold, compared to a 5.9-nm range value and IDC value of 0.008 in 12-nm DNA trench width (in 16.8-nm pitch CNT arrays). The angular deviations for the assembled CNTs were

less than 2° . Under the optimized buffer conditions (supplementary text S1.4), the assembly yields were over 95% (figs. S20, S22, and S24).

The synergy between electrostatic repulsions and DNA hybridization, enabled by the spatial confinement of nanotrenches, helped to eliminate the CNT assembly disorders. In the absence of DNA hybridization, CNTs could not be assembled within the DNA nanotrenches because of the electrostatic repulsions between the negatively charged CNTs and nanotrench sidewalls. The hybridization between DNA handles within the nanotrenches and the DNA antihandles wrapping around CNTs stabilized CNTs within the DNA nanotrenches and resulted in an assembly yield $>95\%$. The absence of effective DNA hybridizations in misaligned CNTs eliminated the assembly disorder by the electrostatic repulsions. The correctly assembled CNTs spatially shielded the DNA handles beneath from being accessed by other CNTs and repelled one another because of negative surface charge. Even for DNA nanotrenches (width from 6 to 12 nm) more than twofold larger than the diameter of single CNTs, we did not observe CNT bundling within individual trenches and achieved an IDC value of 0.001.

Microliter assembly solution at sub-10 pM template concentration simultaneously provided millions of assembled CNT arrays at evenly spaced pitches, demonstrating the scalability of SHINE. We further tested using thermal annealing to remove DNA templates (figs. S27 and S28) and constructed proof-of-concept transistors from parallel CNT arrays (fig. S28). The thermal decomposition of DNAs produced residual contaminations around CNTs that adversely affected the transistor performance. Thus, both low on-state current and large subthreshold swing values were recorded. By contrast, improving interface cleanliness for SHINE promotes transport performance comparable with chemical vapor

deposition-grown or polymer-wrapped CNT arrays in a follow-up study (32). Additionally, using purer semiconducting CNTs may further improve performance.

REFERENCES AND NOTES

1. G. S. Tulevski *et al.*, *ACS Nano* **8**, 8730–8745 (2014).
2. Z. Hu *et al.*, *Nat. Nanotechnol.* **11**, 559–565 (2016).
3. Q. Cao *et al.*, *Nat. Nanotechnol.* **8**, 180–186 (2013).
4. Q. Cao, S.-J. Han, G. S. Tulevski, *Nat. Commun.* **5**, 5071 (2014).
5. G. J. Brady *et al.*, *Sci. Adv.* **2**, e1601240 (2016).
6. X. He *et al.*, *Nat. Nanotechnol.* **11**, 633–638 (2016).
7. J. Wu *et al.*, *Small* **9**, 4142–4148 (2013).
8. S.-P. Han, H. T. Maune, R. D. Barish, M. Bockrath, W. A. Goddard 3rd, *Nano Lett.* **12**, 1129–1135 (2012).
9. A. Mangalum, M. Rahman, M. L. Norton, *J. Am. Chem. Soc.* **135**, 2451–2454 (2013).
10. G. J. Brady, K. R. Jinkins, M. S. Arnold, *J. Appl. Phys.* **122**, 124506 (2017).
11. M. M. Shulaker *et al.*, “High-performance carbon nanotube field-effect transistors,” in *2014 IEEE International Electron Devices Meeting (IEEE)*, (2014), pp. 33.6.1–33.6.4.
12. N. C. Seeman, *J. Theor. Biol.* **99**, 237–247 (1982).
13. N. C. Seeman, *Nature* **421**, 427–431 (2003).
14. P. W. K. Rothmund, *Nature* **440**, 297–302 (2006).
15. S. M. Douglas *et al.*, *Nature* **459**, 414–418 (2009).
16. Y. Ke, L. L. Ong, W. M. Shih, P. Yin, *Science* **338**, 1177–1183 (2012).
17. Y. Ke *et al.*, *Nat. Chem.* **6**, 994–1002 (2014).
18. S. P. Surwade *et al.*, *J. Am. Chem. Soc.* **135**, 6778–6781 (2013).
19. X. Liu *et al.*, *Nature* **559**, 593–598 (2018).
20. Z. Jin *et al.*, *Nat. Commun.* **4**, 1663 (2013).
21. A. Kuzyk *et al.*, *Nature* **483**, 311–314 (2012).
22. P. Zhan *et al.*, *Angew. Chem. Int. Ed.* **57**, 2846–2850 (2018).
23. J. B. Knudsen *et al.*, *Nat. Nanotechnol.* **10**, 892–898 (2015).
24. H. T. Maune *et al.*, *Nat. Nanotechnol.* **5**, 61–66 (2010).
25. H. Pei *et al.*, *J. Am. Chem. Soc.* **141**, 11923–11928 (2019).
26. See supplementary materials.
27. M. Zheng *et al.*, *Nat. Mater.* **2**, 338–342 (2003).
28. Z. Zhao, Y. Liu, H. Yan, *Org. Biomol. Chem.* **11**, 596–598 (2013).
29. W. Sun *et al.*, *Science* **346**, 1258361 (2014).
30. *The International Technology Roadmap for Semiconductors: 2013*; www.semiconductors.org/resources/2013-international-technology-roadmap-for-semiconductors-itrs/.
31. G. Hills *et al.*, *IEEE Trans. NanoTechnol.* **17**, 1259–1269 (2018).
32. M. Zhao *et al.*, *Science* **368**, 878–881 (2020).

ACKNOWLEDGMENTS

The authors acknowledge valuable discussions with W. L. Wilson at the Center for Nanoscale Systems of Harvard University. **Funding:** This work is supported by NSF (CMMI-1333215, CMMI-1344915,

CBET-1729397), ONR (N00014-14-1-0610, N00014-16-1-2410, N00014-18-1-2549), AFOSR (MURI FATE, FA9550-15-1-0514), and Molecular Robotics Initiative from Wyss Institute to P.Y. J.K.S., J.A.F., and M.Z. acknowledge the NIST internal fund for support. **Author contributions:** W.S. conceived, designed, and conducted the study and wrote the manuscript; J.S. designed and conducted the study and wrote the manuscript. Z. Zhao designed and conducted the study. N.A., C.R., J.T., and T.T. fabricated the FETs, characterized the transport performance, and analyzed the data. T.C. and Z. Zhou conducted the experiments and analyzed the data. J.K.S., J.A.F., and M.Z. prepared the DNA-wrapped CNTs and analyzed the data; T.S. analyzed the data and wrote the manuscript. S.-J.H. supervised FET study. W.M.S. contributed to study supervision. H.T.M. designed, conducted, and supervised FET study and wrote the paper. P.Y. conceived and supervised the study and wrote the paper. All authors reviewed, edited, and approved the manuscript. **Competing interests:** A patent based on this work was issued to W.S., J.S. and P.Y. **Data and materials availability:** All data needed to evaluate the conclusions in the paper are present in the paper or the supplementary materials.

SUPPLEMENTARY MATERIALS

science.sciencemag.org/content/368/6493/874/suppl/DC1
Materials and Methods
Supplementary Text
Figs. S1 to S28
References (33–37)

5 October 2019; accepted 9 April 2020
10.1126/science.aaz7440

Precise pitch-scaling of carbon nanotube arrays within three-dimensional DNA nanotrenches

Wei Sun, Jie Shen, Zhao Zhao, Noel Arellano, Charles Rettner, Jianshi Tang, Tianyang Cao, Zhiyu Zhou, Toan Ta, Jason K. Streit, Jeffrey A. Fagan, Thomas Schaus, Ming Zheng, Shu-Jen Han, William M. Shih, Hareem T. Maune and Peng Yin

Science **368** (6493), 874-877.
DOI: 10.1126/science.aaz7440

DNA bricks build nanotube transistors

Semiconducting carbon nanotubes (CNTs) are an attractive platform for field-effect transistors (FETs) because they potentially can outperform silicon as dimensions shrink. Challenges to achieving superior performance include creating highly aligned and dense arrays of nanotubes as well as removing coatings that increase contact resistance. Sun *et al.* aligned CNTs by wrapping them with single-stranded DNA handles and binding them into DNA origami bricks that formed an array of channels with precise intertube pitches as small as 10.4 nanometers. Zhao *et al.* then constructed single and multichannel FETs by attaching the arrays to a polymer-templated silicon wafer. After adding metal contacts across the CNTs to fix them to the substrate, they washed away all of the DNA and then deposited electrodes and gate dielectrics. The FETs showed high on-state performance and fast on-off switching.

Science, this issue p. 874, p. 878

ARTICLE TOOLS

<http://science.sciencemag.org/content/368/6493/874>

SUPPLEMENTARY MATERIALS

<http://science.sciencemag.org/content/suppl/2020/05/20/368.6493.874.DC1>

REFERENCES

This article cites 35 articles, 6 of which you can access for free
<http://science.sciencemag.org/content/368/6493/874#BIBL>

PERMISSIONS

<http://www.sciencemag.org/help/reprints-and-permissions>

Use of this article is subject to the [Terms of Service](#)

Science (print ISSN 0036-8075; online ISSN 1095-9203) is published by the American Association for the Advancement of Science, 1200 New York Avenue NW, Washington, DC 20005. The title *Science* is a registered trademark of AAAS.

Copyright © 2020 The Authors, some rights reserved; exclusive licensee American Association for the Advancement of Science. No claim to original U.S. Government Works